Journal of Power Sources 195 (2010) 6411–6419

Contents lists available at ScienceDirect

Journal of Power Sources

journal homepage: www.elsevier.com/locate/jpowsour

Effect of Fe substitution on the structure and properties of $LnBaCo_{2-x}Fe_xO_{5+\delta}$ (Ln = Nd and Gd) cathodes

Y.N. Kim, J.-H. Kim, A. Manthiram*

Electrochemical Energy Laboratory & Materials Science and Engineering Program, University of Texas at Austin, Austin, TX 78712, USA

ARTICLE INFO

Article history:
Received 1 March 2010
Received in revised form 30 March 2010
Accepted 31 March 2010
Available online 9 April 2010

Keywords:
Solid oxide fuel cells
Cathodes
Layered perovskite
Fe substitution
Oxygen reduction reaction

ABSTRACT

The effect of Fe substitution for Co on the crystal chemistry, thermal and electrical properties, and catalytic activity for oxygen reduction reaction of the layered $LnBaCo_{2-x}Fe_xO_{5+\delta}$ (Ln = Nd and Gd) perovskite has been investigated. The air-synthesized $LnBaCo_{2-x}Fe_xO_{5+\delta}$ samples exhibit structural change with increasing Fe content from tetragonal ($0 \le x \le 1$) to cubic ($1.5 \le x \le 2$) for the Ln = Nd system and from orthorhombic ($x = 0$) to tetragonal ($0.5 \le x \le 1$) for the Ln = Gd system. The thermal expansion coefficient (TEC) and electrical conductivity decrease with increasing Fe content in $LnBaCo_{2-x}Fe_xO_{5+\delta}$. While the substitution of a small amount of Fe ($x = 0.5$) for Co leads to slightly improved performance in solid oxide fuel cells (SOFC), larger Fe contents ($x \ge 1.0$) deteriorate the fuel cell performance. In the Ln = Gd system, the better performance of the $x = 0.5$ sample is partly due to the improved chemical stability with the LSGM electrolyte at high temperatures. With an acceptable electrical conductivity of >100 S cm^{-1} at 800 °C, the $x = 0.5$ sample in the $LnBaCo_{2-x}Fe_xO_{5+\delta}$ (Ln = Nd and Gd) system offers promising mixed oxide-ion and electronic conducting (MIEC) properties.

1. Introduction

Solid oxide fuel cells (SOFC) offer the advantages of employing less expensive catalysts compared to the Pt catalyst used in proton exchange membrane fuel cells and direct use of hydrocarbon fuels without requiring external fuel reforming due to the high operating temperature. However, the conventional high operating temperatures of 800–1000 °C lead to interfacial reactions and thermal expansion mismatch among the components and limitations in the choice of electrode and interconnect materials. These problems have prompted a lowering of the operating temperature to an intermediate range of 500–800 °C, but the poor oxygen reduction reaction (ORR) kinetics of the conventional $La_{1-x}Sr_xMnO_3$ perovskite cathode remains a major obstacle for the intermediate temperature SOFC (IT-SOFC) [1,2]. In this regard, mixed oxide-ion and electronic conducting (MIEC) oxides with perovskite or perovskite-related structures have been widely investigated as alternative cathode materials.

Among the various MIEC oxides, the layered $LnBaCo_2O_{5+\delta}$ (Ln = lanthanide) perovskite has drawn extensive attention in recent years due to the wide variations in oxygen contents ($5+\delta$) and promising MIEC properties. The $LnBaCo_2O_{5+\delta}$ oxides have the Ln–O and Ba–O layers alternating along the *c*-axis, and the difference in the ionic radii between the Ln^{3+} and Ba^{2+} ions plays a dominant role in determining the oxygen content values and the crystal structure [3,4]. Interestingly, the oxygen vacancies are localized in the LnO layer and show an ordering along the *b*-axis at $\delta \sim 0.5$, which is accompanied by a phase transition from tetragonal to orthorhombic structure [5,6]. Also, $PrBaCo_2O_{5+\delta}$ has been found to show good surface exchange kinetics comparable to those of disordered perovskite oxides [7].

The promising MIEC properties of $LnBaCo_2O_{5+\delta}$ (Ln = lanthanide) have stimulated an exploration of their application as cathodes in SOFC. For instance, recent characterization of the high-temperature properties of the $LnBaCo_2O_{5+\delta}$ (Ln = La, Nd, Sm, Gd, and Y) oxides have revealed a decrease in electrical conductivity, thermal expansion coefficient (TEC), and catalytic activity for ORR in SOFC with decreasing size of the Ln^{3+} ions from Ln = La to Y [8]. Although the Ln = Nd sample showed good cathode performance comparable to that of the $La_{0.5}Ba_{0.5}CoO_{3-\delta}$ disordered perovskite, it still suffers from a high TEC value. In addition, the Ln = Gd and Y samples were chemically unstable in contact with the electrolytes at high temperatures. Substitution of Sr for Ba was found to improve the chemical stability of the $GdBa_{1-x}Sr_xCo_2O_{5+\delta}$ cathodes with improved catalytic activity in SOFC [3]. However, the Sr substitution exhibited a side effect of increasing the TEC values due to the increasing Co^{3+} content, which undergoes spin-state transition and causes consequent lattice expansion.

With an aim to lower the TEC and maximize the electrochemical performance, we present here the synthesis and characterization

* Corresponding author. Tel.: +1 512 471 1791; fax: +1 512 471 7681.
E-mail address: rmanth@mail.utexas.edu (A. Manthiram).

0378-7753/$ – see front matter © 2010 Elsevier B.V. All rights reserved.
doi:10.1016/j.jpowsour.2010.03.100

of the $LnBaCo_{2-x}Fe_xO_{5+\delta}$ (Ln = Nd and Gd) oxides as cathode materials for IT-SOFC. The effects of Fe substitution for Co on the crystal chemistry, oxygen content, electrical conductivity, TEC, chemical stability in contact with the electrolyte, polarization conductance, and catalytic activity for ORR in SOFC are presented.

2. Experimental

The $LnBaCo_{2-x}Fe_xO_{5+\delta}$ (Ln = Nd, Gd) oxides were synthesized by conventional solid-state reaction methods. Required amounts of Nd_2O_3, Gd_2O_3, $BaCO_3$, Co_3O_4, and Fe_2O_3 were thoroughly mixed in an agate mortar and pestle and calcined at 1000 °C for 12 h in air. The calcined powders were then ground, pressed into pellets, and sintered at 1200 °C for 12 h ($0.0 \le x \le 2.0$) in air. The resulting powders were annealed at 900 °C for 6 h in air, followed by slow cooling to room temperature at a rate of 1 °C min^{-1} in air to maximize the oxygen content. The $La_{0.8}Sr_{0.2}Ga_{0.8}Mg_{0.2}O_{2.8}$ (LSGM) electrolyte disks were prepared by firing required amounts of La_2O_3, $SrCO_3$, Ga_2O_3, and MgO at 1100 °C for 5 h, followed by pelletizing and sintering at 1500 °C for 10 h. The $Ce_{0.9}Gd_{0.1}O_{1.95}$ (GDC) and $La_{0.4}Ce_{0.6}O_{1.8}$ (LDC) powders were synthesized by the glycine-nitrate combustion method [9,10] as described below. Required amounts of Gd_2O_3 (or La_2O_3) and $Ce(NH_4)_2(NO_3)_6$ were dissolved in dilute HNO_3 solution containing glycine (NH_2CH_2COOH). On heating the mixture on a hot plate, a viscous gel was formed as the solvent evaporated, followed by its vigorous auto-ignition. The resulting voluminous powder was then fired at 600 °C for 2 h to burn out residual carbon. For the anode, the GDC powder thus obtained was mixed with NiO (Ni:GDC = 70:30 vol%) by ball-milling in ethanol for 48 h.

The synthesized materials were characterized by X-ray diffraction (XRD), and the XRD data were refined with the Rietveld method with the Fullprof program [11]. The average oxidation state of (Co, Fe) and the room temperature oxygen content values were determined by iodometric titration [12]. Thermogravimetric analysis (TGA) was performed with a PerkinElmer Series 7 thermal analysis system. The TGA experiments were carried out from room temperature to 900 °C with a heating/cooling rate of 3 °C min^{-1}. The TEC data were obtained with a Linseis thermal analysis system. The TECs of the specimens were measured for three consecutive heating/cooling cycles in the temperature range of 80–900 °C with a heating/cooling rate of 3 °C min^{-1} and intermediate dwellings at 900 °C for 1 h. Electrical conductivity of the $LnBaCo_{2-x}Fe_xO_{5+\delta}$ (Ln = Nd and Gd) pellets were measured with a four-probe dc method using a Van der Pauw configuration [13,14] in the temperature range of 40–900 °C. Chemical stability of the $LnBaCo_{2-x}Fe_xO_{5+\delta}$ (Ln = Nd and Gd) samples with the LSGM electrolytes was evaluated by heating a mixture of the $LnBaCo_{2-x}Fe_xO_{5+\delta}$ and LSGM powders (1:1 wt ratio) at 1050 °C for 3 h in air.

Electrochemical performances of the $LnBaCo_{2-x}Fe_xO_{5+\delta}$ (Ln = Nd and Gd) cathodes for ORR were evaluated with LSGM electrolyte-supported single SOFCs. The NiO–GDC cermet anode powders were mixed with an organic binder (Heraeus V006) to form slurries and then applied onto the surface of dense LSGM (520 μm thickness) by screen printing, followed by firing at 1300 °C for 0.5 h. To prevent the formation of $LaNiO_3$ or La_2NiO_4 at the anode|LSGM interface, the LDC buffer layer was applied by screen printing between the anode and the electrolyte [15]. Similarly, a composite layer consisting of $LnBaCo_{2-x}Fe_xO_{5+\delta}$ (Ln = Nd and Gd) and LSGM (1:1 wt ratio) was first prepared by screen printing onto the cathode side of the LSGM electrolyte and heated at 1050 °C for 3 h. The $LnBaCo_{2-x}Fe_xO_{5+\delta}$ (Ln = Nd and Gd) cathode layer was subsequently screen printed onto the $LnBaCo_{2-x}Fe_xO_{5+\delta}$ + LSGM composite layer and heated at 1050 °C for 3 h. In order to keep the particle size and microstructure similar, single cell with the Fe-free cathode ($x = 0$) was also prepared by adopting a lower heating temperature of 1000 °C for 3 h. The intermediate $LnBaCo_{2-x}Fe_xO_{5+\delta}$ + LSGM composite layer ensures good interfacial contact between the LSGM electrolyte and the $LnBaCo_{2-x}Fe_xO_{5+\delta}$ cathode. Pt meshes and wires were attached to each electrode with an area of 0.25 cm^2 using Pt paste as a current collector. Pt reference electrode was placed at a distance of 5 mm from the cathode. During the SOFC operation, humidified H_2 (~3% H_2O at 25 °C) and air were supplied as fuel and oxidant, respectively, at a rate of 100 cm^3 min^{-1}. The polarization resistance (R_p) of the $LnBaCo_{2-x}Fe_xO_{5+\delta}$ (Ln = Nd and Gd) cathodes in the LSGM-supported SOFCs was measured at different temperatures by ac impedance spectroscopy (Solartron 1260 FRA) at open circuit voltage (OCV). After the SOFC performance tests, the microstructures of the $LnBaCo_{2-x}Fe_xO_{5+\delta}$ (Ln = Nd and Gd) cathodes were observed with a JEOL JSM-5610 scanning electron microscope (SEM).

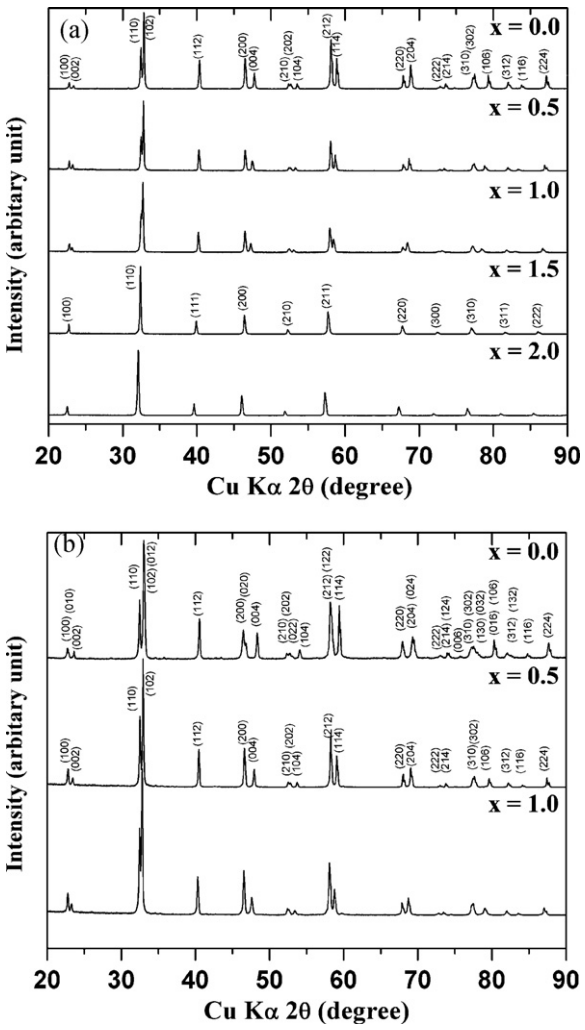

Fig. 1. XRD patterns of the (a) $NdBaCo_{2-x}Fe_xO_{5+\delta}$ and (b) $GdBaCo_{2-x}Fe_xO_{5+\delta}$ samples with various Fe contents.

3. Results and discussion

3.1. Crystal structure of $LnBaCo_{2-x}Fe_xO_{5+\delta}$

Fig. 1(a) shows the room temperature XRD patterns of the $NdBaCo_{2-x}Fe_xO_{5+\delta}$ ($0 \le x \le 2.0$) system. For $0 \le x \le 1.0$, the XRD patterns of the $NdBaCo_{2-x}Fe_xO_{5+\delta}$ samples could be indexed on the basis of a tetragonal structure with the space group *P*4/*mmm*. How-

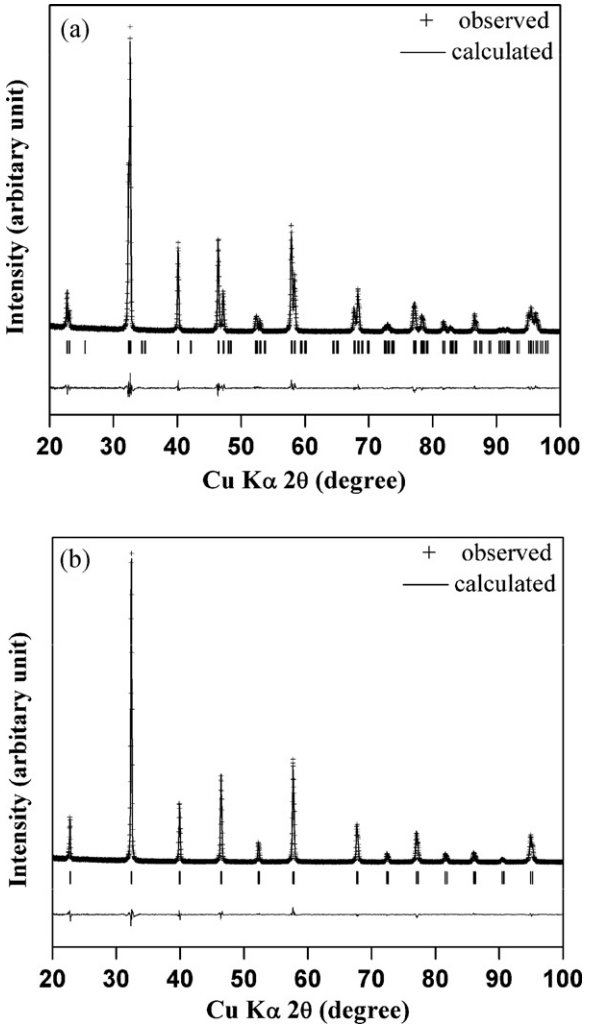

Fig. 2. Observed and calculated XRD profiles and the difference between them for the (a) $NdBaCo_{1.0}Fe_{1.0}O_{5+\delta}$ and (b) $NdBaCo_{0.5}Fe_{1.5}O_{5+\delta}$ samples. The vertical bars show the calculated peak positions.

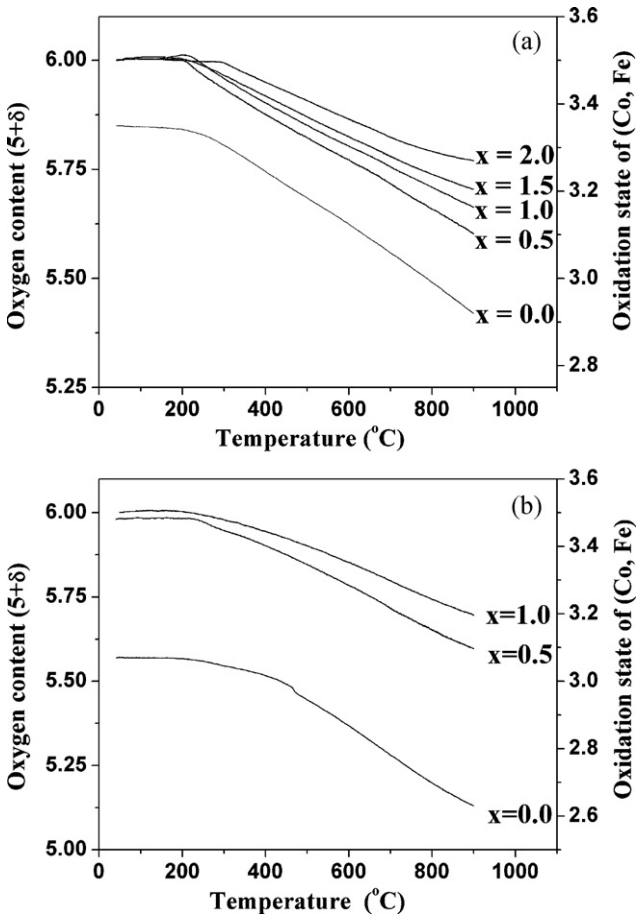

Fig. 3. Variations of the oxygen content and the oxidation state of (Co, Fe) in the (a) $NdBaCo_{2-x}Fe_xO_{5+\delta}$ and (b) $GdBaCo_{2-x}Fe_xO_{5+\delta}$ samples with temperature in air.

ever, the crystal structure changes from tetragonal to cubic (space group: *Pm*–3*m*) with increasing Fe content ($x = 1.5$ and 2.0). Fig. 2 gives the Rietveld refinement data of the $x = 1.0$ and 1.5 samples that were obtained based on, respectively, the space groups *P*4/*mmm* and *Pm*–3*m*. There is good agreement between the observed and calculated profiles, and the quality of the refinements and atomic positions are listed in Table 1. These results reveal that the $x = 1.5$ and 2.0 samples prefer to be disordered as $Nd_{1/2}Ba_{1/2}Co_{1-x/2}Fe_{x/2}O_3$ rather than ordered $NdBaCo_{2-x}Fe_xO_{5+\delta}$ in air. It has been reported that the ordered $LnBaFe_2O_{5+\delta}$ (Ln = lanthanide) perovskite with the tetragonal structure could be obtained only in reducing atmosphere [16,17]. In addition, the $DyBaFe_2O_{5+\delta}$ ordered perovskite synthesized in such reducing atmosphere has been observed to exhibit phase decomposition into disordered perovskite on exposing it oxidative atmosphere at 1000 °C [16].

Fig. 1(b) shows the XRD patterns of the $GdBaCo_{2-x}Fe_xO_{5+\delta}$ ($0 \le x \le 1$) system. At higher Fe contents with $x > 1.0$, the XRD pat-

Table 1
Room temperature atomic positions in the $LnBaCo_{2-x}Fe_xO_{5+\delta}$ (Ln = Nd and Gd) oxides annealed at 900 °C for 6 h, followed by slow cooling at a rate of 1 °C/min in air. For the tetragonal structure with the space group of *P*4/*mmm*, the atomic positions are Ln (0,0,1/2), Ba (0,0,0), (Co, Fe) (1/2,1/2,*z*), O1 (1/2,1/2,0), O2 (1/2,0,*z*), and O3 (1/2,1/2,1/2). For the orthorhombic structure with the space group of *Pmmm*, the atomic positions are Gd (1/2,*y*,1/2), Ba (1/2,*y*,0), (Co1) (0,1/2,*z*), (Co2) (0,0,*z*), O1 (0,0,0), O2 (0,1/2,0), O3 (0,1/2,1/2), O4 (0,0,1/2), O5 (1/2,0,z), O6 (1/2,1/2,*z*), and O7 (0,*y*,*z*).

Ln = Nd	Tetragonal *P*4/*mmm*	$x = 0.0$	$x = 0.5$	$x = 1.0$	Cubic *Pm*–3*m*	$x = 1.5$	$x = 2.0$
	(Co, Fe)(*z*)	0.249 (1)	0.252 (1)	0.250 (1)			
	O2(*z*)	0.278 (1)	0.279 (1)	0.280 (1)			
	χ^2	3.01	1.67	1.58	χ^2	1.77	2.00
	R_{Bragg}	4.07	4.62	2.50	R_{Bragg}	2.35	3.58

Ln = Gd	Orthorhombic *Pmmm*	$x = 0.0$			Tetragonal *P*4/*mmm*	$x = 0.5$	$x = 1.0$
	Gd (*y*)	0.272 (1)	O6 (*z*)	0.266 (5)	(Co, Fe)(*z*)	0.249 (1)	0.251 (1)
	Ba (*y*)	0.250 (1)	O7 (*y*)	0.244 (2)	O2(*z*)	0.289 (1)	0.286 (1)
	Co1 (*z*)	0.250 (1)	O7 (*z*)	0.279 (3)	χ^2	2.44	2.40
	Co2 (*z*)	0.250 (1)	χ^2	3.26	R_{Bragg}	4.32	3.34
	O5 (*z*)	0.307 (4)	R_{Bragg}	4.43			

Table 2
Structural parameters, chemical analysis data, and TEC of the $LnBaCo_{2-x}Fe_xO_{5+\delta}$ (Ln = Nd and Gd) oxides.

Ln	x	Space group	Z	a (Å)	b (Å)	c (Å)	V (Å^3)	Oxidation state of (Co, Fe)	Oxygen content $(5+\delta)$	TEC $\times 10^6$ ($^\circ$C^{-1}) 80–900 °C
Nd	0.0	*P*4/*mmm*	1	3.896	–	7.619	115.65	3.35	5.85	21.5
	0.5	*P*4/*mmm*	1	3.905	–	7.661	116.82	3.50	6.00	20.8
	1.0	*P*4/*mmm*	1	3.912	–	7.704	117.90	3.50	6.00	20.0
	1.5[a]	*Pm*–3*m*	1	3.912	–	–	59.87	–	–	20.7
	2.0[a]	*Pm*–3*m*	1	3.930	–	–	60.70	–	–	18.3
Gd	0.0	*Pmmm*	2	3.877	7.825	7.542	228.81	3.07	5.57	19.9
	0.5	*P*4/*mmm*	1	3.895	–	7.592	115.18	3.49	5.98	19.6
	1.0	*P*4/*mmm*	1	3.903	–	7.643	116.43	3.50	6.00	18.8

[a] Lattice parameter and volume are based on the chemical formula of $Nd_{1/2}Ba_{1/2}Co_{1-x/2}Fe_{x/2}O_3$.

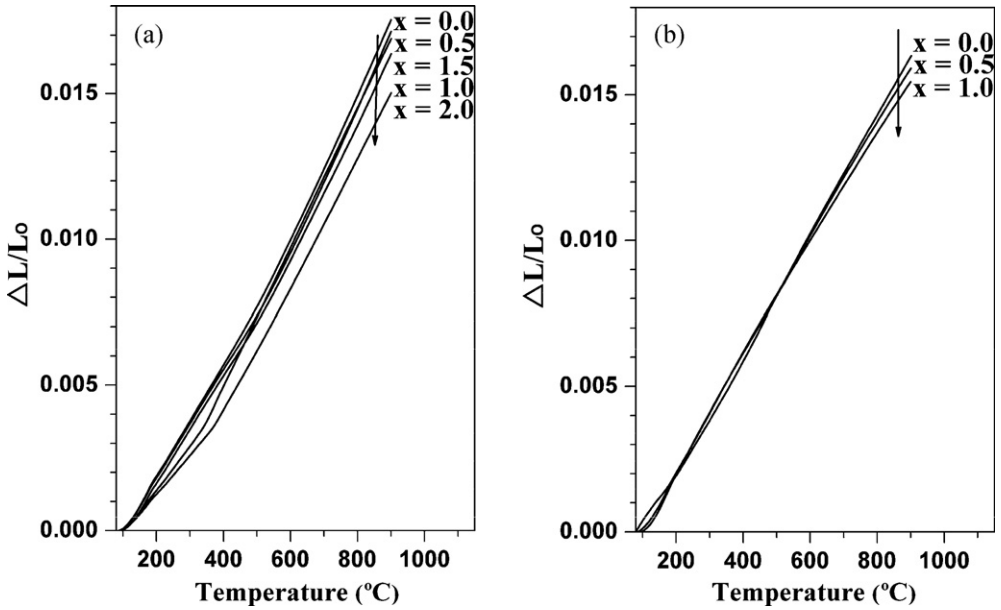

Fig. 4. Thermal expansion ($\Delta L/L_0$) curves of the (a) $NdBaCo_{2-x}Fe_xO_{5+\delta}$ and (b) $GdBaCo_{2-x}Fe_xO_{5+\delta}$ specimens in the temperature range of 80–900 °C in air.

terns show the formation of $GdFeO_3$ impurity phase, indicating a Fe solubility of ~1.0 in the $GdBaCo_{2-x}Fe_xO_{5+\delta}$ system in air. The crystal structure of the $GdBaCo_{2-x}Fe_xO_{5+\delta}$ samples change with increasing Fe content from orthorhombic (space group: *Pmmm*) for $x = 0$ to tetragonal (space group: *P*4/*mmm*) for $x = 0.5$ and 1.0. Their atomic positions and the quality of the Rietveld refinements are given in Table 1.

The data in Table 2 indicate that the lattice parameters and the unit cell volume of the $LnBaCo_{2-x}Fe_xO_{5+\delta}$ increase with increasing Fe content in both the Ln = Nd and Gd systems. This can be explained by the larger ionic radii of $Fe^{3+/4+}$ compared to that of $Co^{3+/4+}$ [18]. Both the oxygen content $(5+\delta)$ and the oxidation state of (Co, Fe) in the $LnBaCo_{2-x}Fe_xO_{5+\delta}$ system increase with Fe content as seen in Table 2. Unfortunately, the oxygen content $(5+\delta)$ of the $LnBaCo_{2-x}Fe_xO_{5+\delta}$ (Ln = Nd and Gd) samples with high Fe contents ($x > 1.0$) could not be determined precisely as the samples were hardly soluble in weakly acidic solutions to be analyzed by the iodometric titration technique. Nevertheless, it will be reasonable to assume that the $x = 1.5$ and 2.0 samples in the Ln = Nd system may have fully occupied oxygen sites with an oxygen content of 6.0 at room temperature like the $x = 1.0$ sample. In the $GdBaCo_{2-x}Fe_xO_{5+\delta}$ system, the higher oxygen content values ($\delta \approx 1.0$) of the $x = 0.5$ and 1.0 samples compared to that of the $x = 0$ sample ($\delta = 0.57$) destroy the ordering of the oxygen vacancies, resulting in a tetragonal structure as seen in Fig. 1(b).

3.2. Thermal and electrical properties of $LnBaCo_{2-x}Fe_xO_{5+\delta}$

Fig. 3 shows the variations of the oxygen content and oxidation state of (Co, Fe) in the $LnBaCo_{2-x}Fe_xO_{5+\delta}$ (Ln = Nd and Gd) system with temperature in air. These curves were derived using the initial oxygen content values determined by the iodometric titration and the TGA data. The room temperature oxygen contents of the $x = 1.5$ and 2.0 samples in the $NdBaCo_{2-x}Fe_xO_{5+\delta}$ system were assumed to be 6.0 based on the oxygen content value of the $x = 0.5$ sample. All the $LnBaCo_{2-x}Fe_xO_{5+\delta}$ samples start to lose oxygen at $T > 200$ °C with a decrease in the oxidation state of (Co, Fe). The data in Fig. 3 reveal that the degree of oxygen loss decreases with increasing Fe content in both the Ln = Nd and Gd systems. A similar trend has also been observed in the disordered $(Ln, Sr)Co_{1-x}Fe_xO_3$ perovskite system [19]. The stronger Fe–O bond compared to the Co–O bond [20] suppresses the oxygen loss on heating the samples with high Fe content.

The thermal expansion behaviors of the $LnBaCo_{2-x}Fe_xO_{5+\delta}$ (Ln = Nd and Gd) specimens at 80–900 °C in air are shown in Fig. 4. At a given temperature, the degree of thermal expansion ($\Delta L/L_0$) decreases with increasing Fe content in both the Ln = Nd and Gd systems. Their average TEC values at 80–900 °C also decrease with increasing Fe content as seen in Table 2. This can be understood by considering the degree of oxygen loss in Fig. 3. The formation of oxygen vacancies is known to increase TEC due to the reduction of (Co, Fe) ions and the consequent lattice expansion in $LnBaCo_{2-x}Fe_xO_{5+\delta}$.

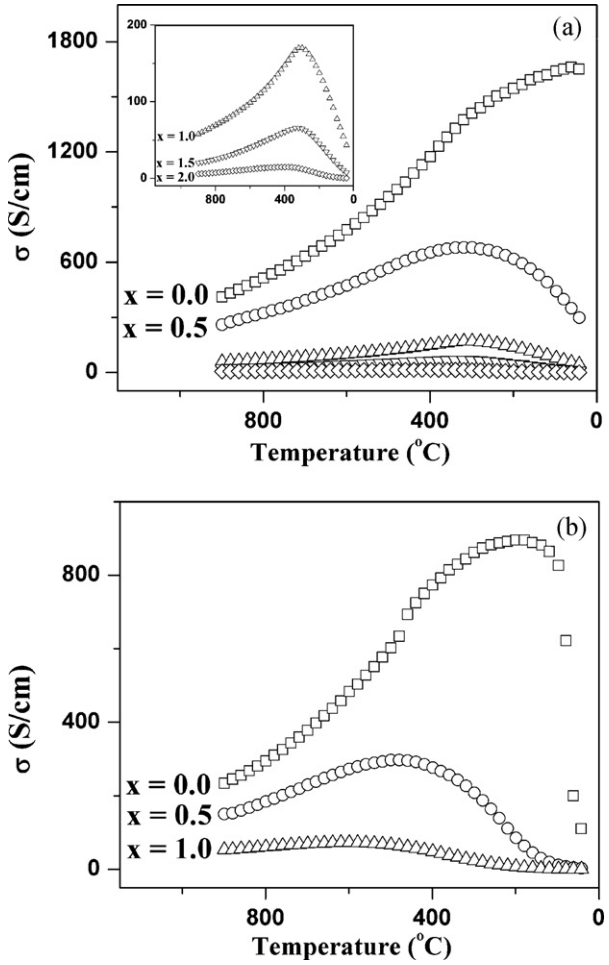

Fig. 5. Variations of the electrical conductivity of the (a) $NdBaCo_{2-x}Fe_xO_{5+\delta}$ and (b) $GdBaCo_{2-x}Fe_xO_{5+\delta}$ specimens with temperature in air.

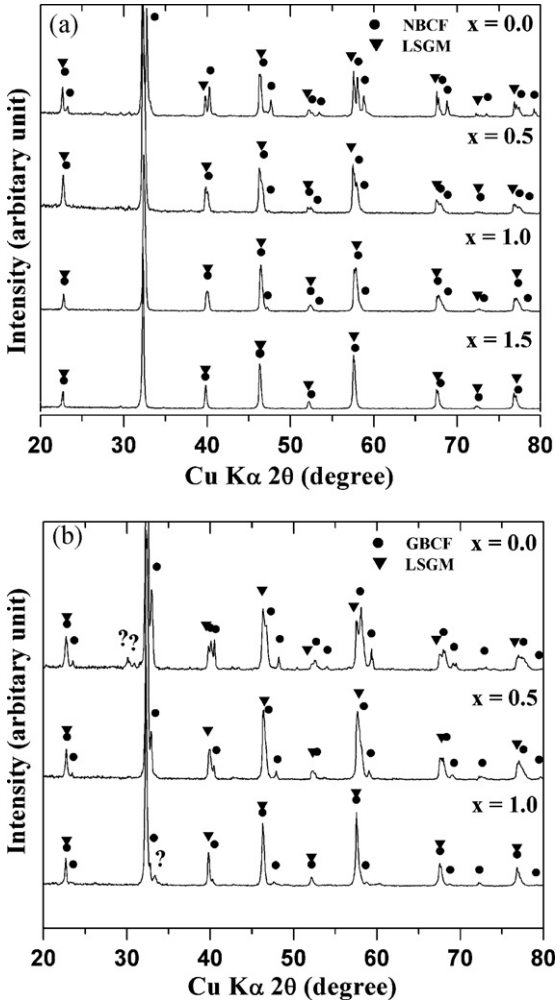

Fig. 6. Chemical stability of the (a) $NdBaCo_{2-x}Fe_xO_{5+\delta}$ and (b) $GdBaCo_{2-x}Fe_xO_{5+\delta}$ samples against LSGM electrolyte. The data were collected after heating a 1:1 mixture of the cathode and LSGM powders at 1050 °C for 3 h in air, followed by recording the XRD patterns at room temperature. The reflections marked with? belong to unknown phases.

Therefore, the decrease in the amount of oxygen loss with increasing Fe content, which originates from the stronger Fe–O bond compared to the Co–O bond, leads to a decrease in TEC with increasing Fe content. In addition, the low-spin to high-spin transition of the Co^{3+} ions with increasing temperature has been reported to be the reason for the abnormally high TEC of cobalt-based perovskite oxides [21,22]. The substitution of high spin $Fe^{3+/4+}$ and the consequent decrease in the Co content in $LnBaCo_{2-x}Fe_xO_{5+\delta}$ also leads to a decrease in TEC with increasing Fe content.

Fig. 5 shows the variations of the electrical conductivity with temperature of the $LnBaCo_{2-x}Fe_xO_{5+\delta}$ (Ln = Nd and Gd) samples. The sudden decrease in the conductivity of $GdBaCo_2O_{5+\delta}$ at $T < 200$ °C is characteristic of a metal-insulator (M-I) transition (Fig. 5(b)), which occurs due to the low-spin to high-spin transition of Co^{3+} ions [23]. This M–I transition becomes less pronounced for $NdBaCo_2O_{5+\delta}$ in Fig. 5(a) due to the increasing oxygen content $(5+\delta)$ and the consequent increase in the oxidation state of Co, which in turn results in an increase in the Co–O covalency and bandwidth [24]. However, both the samples show a decrease in electrical conductivity with increasing temperature at $T > 200$ °C due to the increasing concentration of oxygen vacancies (Fig. 3). At a given temperature, electrical conductivity decreases with increasing Fe content in $LnBaCo_{2-x}Fe_xO_{5+\delta}$ (Ln = Nd and Gd). Unlike the Fe-free samples, the electrical conductivities of the Fe-substituted samples increase gradually with temperature and reach a maximum at ~300 °C for the Ln = Nd and at ~500 °C for the Ln = Gd samples, implying a typical semiconductor behavior. Further increase in temperature decreases the electrical conductivity due to the increasing concentration of oxygen vacancies in $LnBaCo_{2-x}Fe_xO_{5+\delta}$. The formation of oxide-ion vacancies not only decreases the carrier concentration but also perturbs the (Co, Fe)–O–(Co, Fe) periodic potential and introduces carrier localization [24,25].

3.3. Chemical stability and electrochemical performance of $LnBaCo_{2-x}Fe_xO_{5+\delta}$

Chemical stability of the $LnBaCo_{2-x}Fe_xO_{5+\delta}$ sample in contact with the LSGM electrolyte was assessed by heating the mixture at 1050 °C for 3 h. Fig. 6 shows the XRD patterns of the $LnBaCo_{2-x}Fe_xO_{5+\delta}$ (Ln = Nd and Gd) and LSGM mixtures after the heat treatment. The $NdBaCo_{2-x}Fe_xO_{5+\delta}$ samples show no distinct side reaction product from the XRD data in Fig. 6(a). However, the XRD data show impurity peaks at $2\theta \approx 29$–$31°$ for the $x = 0$ sample in the $GdBaCo_{2-x}Fe_xO_{5+\delta}$ system in accordance with an earlier report [3]. Although a slight amount of Fe substitution ($x = 0.5$) suppresses this side reaction, the $x = 1.0$ sample in $GdBaCo_{2-x}Fe_xO_{5+\delta}$ again exhibits a slight impurity peak at $2\theta \approx 34°$.

The electrochemical performances of the $LnBaCo_{2-x}Fe_xO_{5+\delta}$ (Ln = Nd and Gd) cathodes in SOFC for the oxygen reduction reaction was evaluated using LSGM as an electrolyte. Fig. 7 shows the SEM images of the cross sections of the cathode|cathode + LSGM|LSGM

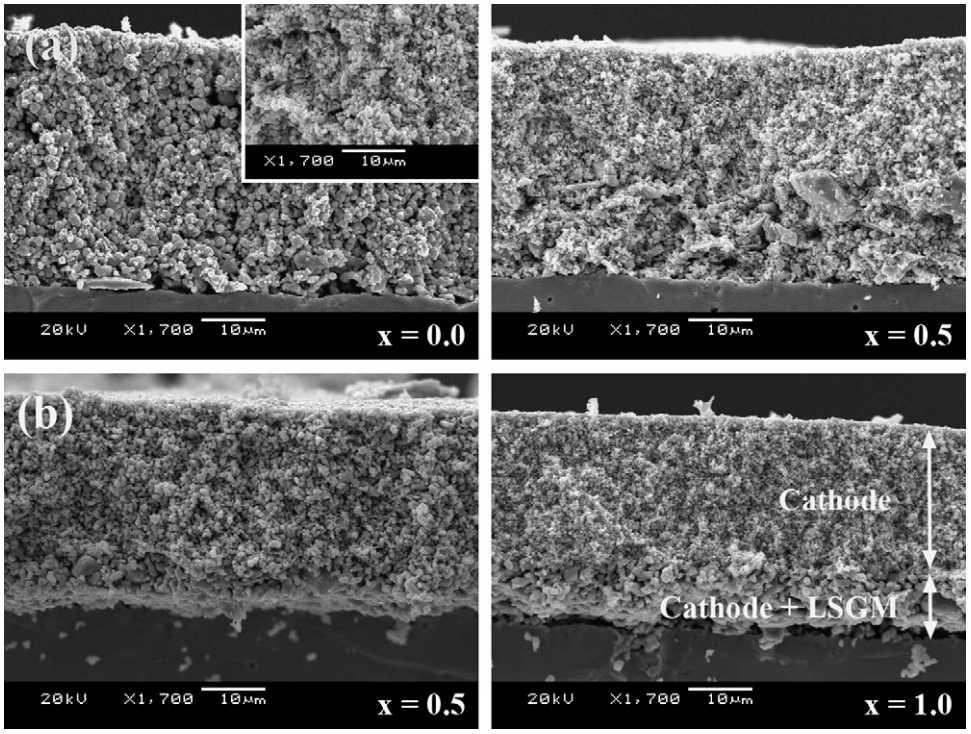

Fig. 7. SEM micrographs showing the cross sections of the cathode|cathode + LSGM|LSGM portion for (a) $NdBaCo_{2-x}Fe_xO_{5+\delta}$ ($x = 0$ and 0.5) and (b) $GdBaCo_{2-x}Fe_xO_{5+\delta}$ ($x = 0.5$ and 1.0) cathodes attached at 1050 °C for 3 h. The insets in (a) and (b) show the $x = 0$ samples (Ln = Nd and Gd) attached at 1000 °C for 3 h.

portion after the SOFC single cell performance tests. The TECs of the $LnBaCo_{2-x}Fe_xO_{5+\delta}$ cathodes (Table 2) are higher than that of the $La_{0.8}Sr_{0.2}Ga_{0.8}Mg_{0.2}O_{2.8}$ (LSGM) electrolyte ($12.4 \times 10^{-6}\,K^{-1}$) [26]. To alleviate the thermal expansion mismatch between the electrolyte and cathode, we introduced the cathode + LSGM composite layer in between the cathode and the LSGM electrolyte. While the bottom of the micrograph indicates a dense LSGM electrolyte, the upper portion shows the porous cathode|cathode + LSGM layers with the total thicknesses of about 30–40 μm. In Fig. 7(a), the Fe-substituted sample ($x = 0.5$) consists of smaller particles compared to the Fe-free sample ($x = 0$) after heating at 1050 °C for 3 h. To minimize the effect of the differences in the cathode microstruc-

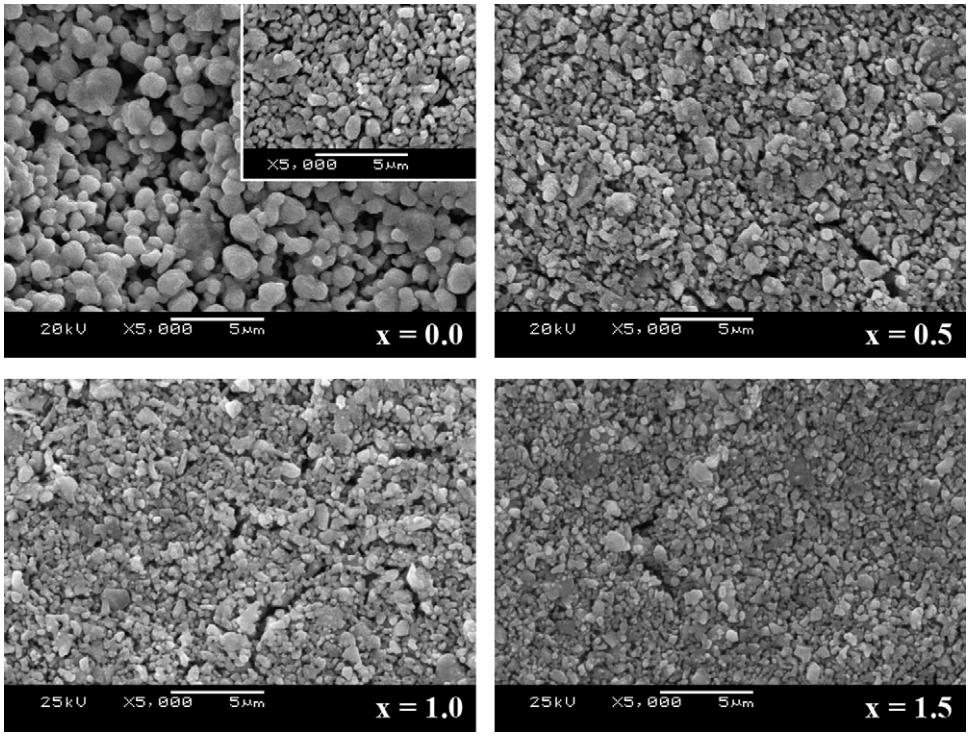

Fig. 8. SEM micrographs showing the surface of the $NdBaCo_{2-x}Fe_xO_{5+\delta}$ ($0 \le x \le 1.5$) cathodes attached at 1050 °C for 3 h. The inset shows the $x = 0$ sample attached at 1000 °C for 3 h.

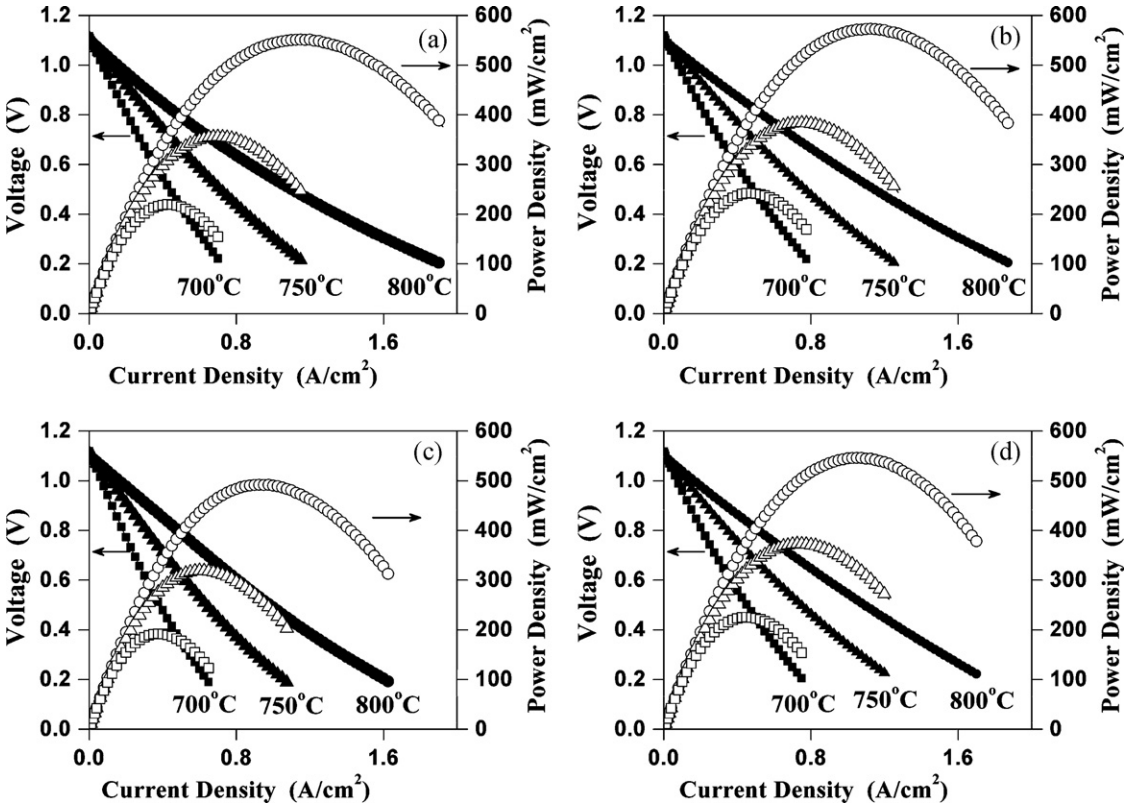

Fig. 9. *I–V* curves (closed symbols) and corresponding power density curves (open symbols) of the $LnBaCo_{2-x}Fe_xO_{5+\delta}$|$LnBaCo_{2-x}Fe_xO_{5+\delta}$ + LSGM|LSGM|LDC|Ni + GDC single cells at 800 °C (square), 750 °C (triangle), and 700 °C (circle): (a) $NdBaCo_2O_{5+\delta}$, (b) $NdBaCo_{1.5}Fe_{0.5}O_{5+\delta}$, (c) $GdBaCo_2O_{5+\delta}$, and (d) $GdBaCo_{1.5}Fe_{0.5}O_{5+\delta}$.

ture on the electrochemical performance, a single cell with the $x = 0$ cathode was also prepared by attaching the cathode at 1000 °C for 3 h instead of at 1050 °C. The resulting $x = 0$ cathode layer (inset in Fig. 7(a)) consists of much smaller particles compared to the $x = 0$ cathode attached at 1050 °C, and the particle size is similar to that of the $x = 0.5$ cathode attached at 1050 °C. Fig. 8 shows the SEM images of the $NdBaCo_{2-x}Fe_xO_{5+\delta}$ cathode surface after the fuel cell test. It is apparent that the particle size decreases with Fe substitution; similar observations were made with the Ln = Gd system as well (not shown here). In Fig. 8, the $x = 0$ cathode attached at 1000 °C for 3 h (inset in Fig. 8) again shows smaller particle size similar to that of the $x = 0.5$ cathode attached at 1050 °C for 3 h.

Fig. 9 shows the current–voltage (*I–V*) curves and corresponding power density curves obtained with the $NdBaCo_{2-x}Fe_xO_{5+\delta}$ and $GdBaCo_{2-x}Fe_xO_{5+\delta}$ cathodes at various temperatures. At a given Fe content, the $NdBaCo_{2-x}Fe_xO_{5+\delta}$ system exhibits higher performance than the $GdBaCo_{2-x}Fe_xO_{5+\delta}$ system. This is in accordance with the reports that fuel cell performance of the $LnBaCo_2O_{5+\delta}$ cathode decreases with decreasing size of Ln^{3+} ions due to the decreasing oxygen bulk diffusion and surface exchange rates [7,8,27]. From the fuel cell performance tests, the variations of the maximum power density with Fe contents at 700, 750, and 800 °C are plotted in Fig. 10. For a comparison, the maximum power densities (at 800 °C) of the $x = 0$ cathodes (Ln = Nd and Gd) attached at 1000 °C for 3 h are also shown in Fig. 10 (see the closed symbols). Despite the smaller particles and the consequent larger surface area, the $x = 0$ cathodes attached at 1000 °C show inferior fuel cell performance compared to those attached at 1050 °C. This can be explained to be due to the poor connectivity between the cathode particles or the electrolyte particles, which provide electron or oxide-ion conducting pathways, respectively, in the composite cathode [28]. Interestingly, the $x = 0.5$ sample shows slightly improved cathode performance compared to the $x = 0$ sample in both the Ln = Nd and Gd systems. However, the maximum power density decreases on increasing the Fe content further with $x \geq 1.0$. Considering the chemical stability data in Fig. 6(b), the lower cathode performances of the $x = 0$ and 1.0 samples, compared to that of the $x = 0.5$ sample in the $GdBaCo_{2-x}Fe_xO_{5+\delta}$ system, could be partly due to the formation of the unknown impurity phase at the $GdBaCo_{2-x}Fe_xO_{5+\delta}$ |LSGM interface.

Total cathode polarization conductance (R_p^{-1}) of the $LnBaCo_{2-x}Fe_xO_{5+\delta}$ (Ln = Nd and Gd) were also measured by AC impedance spectroscopy with temperature in air. In Fig. 11,

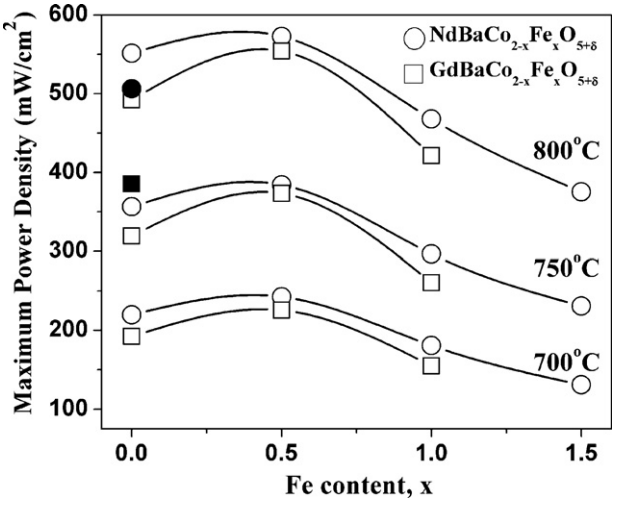

Fig. 10. Variations of the maximum power density with Fe content in $LnBaCo_{2-x}Fe_xO_{5+\delta}$ (Ln = Nd and Gd) at 800, 750, and 700 °C with the cathodes attached at 1050 °C for 3 h. The maximum power densities obtained at 800 °C for the $x = 0$ cathodes attached at 1000 °C for 3 h are indicated by closed square for Ln = Nd and closed circle for Ln = Gd.

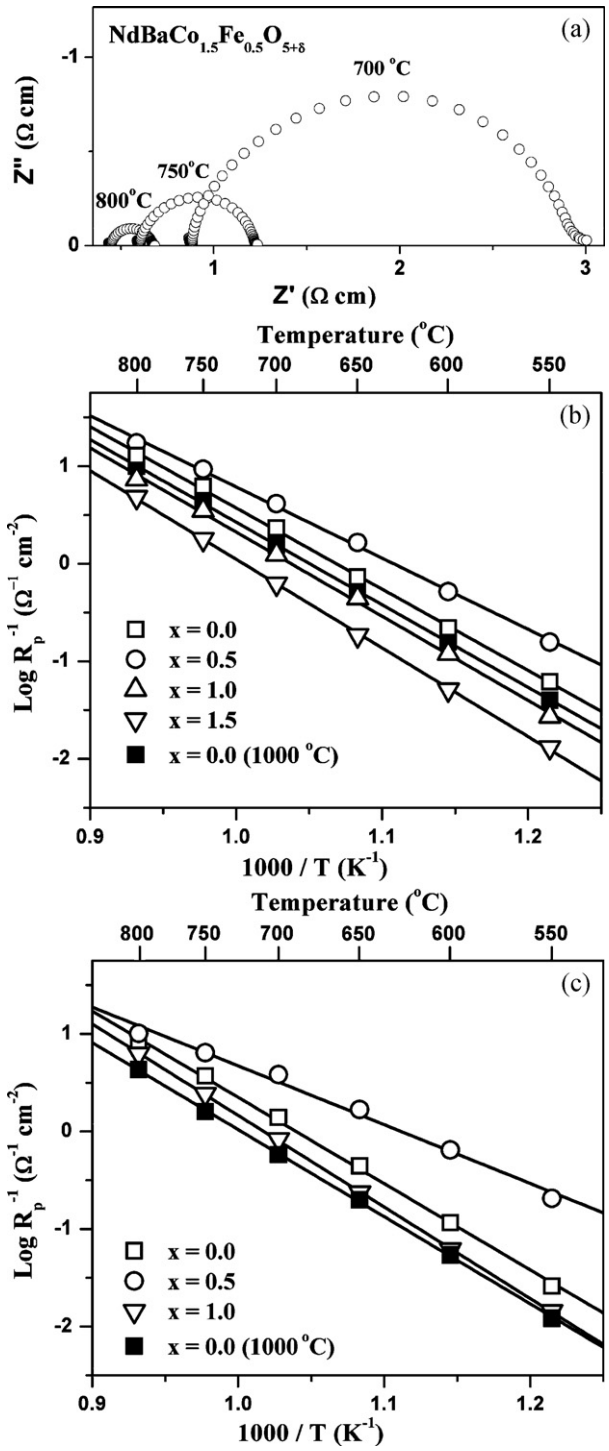

Fig. 11. (a) Representative area-normalized AC impedance spectra obtained with the $NdBaCo_{1.5}Fe_{0.5}O_{5+\delta}$ cathode at different temperatures, and variations of the total polarization conductance (R_p^{-1}) of the (b) $NdBaCo_{2-x}Fe_xO_{5+\delta}$ and (c) $GdBaCo_{2-x}Fe_xO_{5+\delta}$ cathodes with temperature. The data obtained with the cathodes attached at 1050 °C for 3 h are indicated with open symbols and those obtained with the $x = 0$ cathodes attached at 1000 °C for 3 h are indicated with closed squares.

the R_p^{-1} increases from $x = 0$ to $x = 0.5$ and then decreases with further increase in Fe content, which is consistent with the SOFC performance data in Figs. 9 and 10. In accordance with the SOFC performance data, the $x = 0$ cathodes attached at 1000 °C show lower cathode polarization conductances compared to those attached at 1050 °C in both the Ln = Nd and Gd systems. From the Arrhenius plots of the cathode polarization conductance, the activation energies were calculated to be 1.68, 1.45, 1.71, and 1.80 eV, respectively, for the $x = 0$, 0.5, 1.0, and 1.5 samples in the $NdBaCo_{2-x}Fe_xO_{5+\delta}$ system. Similarly, the activation energies were calculated to be 1.75, 1.20, and 1.86 eV, respectively, for the $x = 0$, 0.5, and 1.0 samples in the $GdBaCo_{2-x}Fe_xO_{5+\delta}$ system. As seen, the $x = 0.5$ sample shows the lowest activation energy for the cathode polarization conductance in both the Ln = Nd and Gd systems, resulting in a maximum power density at $x = 0.5$.

The layered $LnBaCo_{2-x}Fe_xO_{5+\delta}$ (Ln = Nd and Gd) perovskite oxides show a decrease in TEC and electrochemical performance with increasing Fe content (except for $x = 0.5$), which is similar to those observed in disordered perovskite systems. However, the degree of decrease in TEC with Fe content in the layered $LnBaCo_{2-x}Fe_xO_{5+\delta}$ (Ln = Nd and Gd) oxides is lower than that found with the disordered perovskite oxides such as $Nd_{0.6}Sr_{0.4}Co_{1-x}Fe_xO_{3-\delta}$ [19]. This could be partly related to the larger ionicity of the Ba–O bonds in the former compared to the Sr–O bonds in the latter as the ionic bonds generally exhibit larger thermal expansion than the covalent bonds. The decreasing electrochemical performance of the $LnBaCo_{2-x}Fe_xO_{5+\delta}$ (Ln = Nd and Gd) cathodes with increasing Fe substitution could be attributed to the decreasing total electrical conductivity (Fig. 5) and sluggish oxygen diffusion in the bulk as has been found with the disordered perovskite systems [29,30]. However, the $x = 0.5$ samples show slightly improved cathode performances (Figs. 9–11) compared to the $x = 0$ samples attached at 1000 °C and 1050 °C for 3 h. In the case of Ln = Gd system, the higher performance of the $x = 0.5$ sample compared to those of the $x = 0$ and 1.0 is partly due to the improved chemical stability in contact with the LSGM electrolyte at high temperatures (Fig. 6). With an acceptable electrical conductivity of > 100 S cm^{-1} at 800 °C, the $x = 0.5$ samples in the $LnBaCo_{2-x}Fe_xO_{5+\delta}$ (Ln = Nd and Gd) system offer attractive MIEC properties, and our future work will focus on investigating this further.

4. Conclusions

With an aim to develop new cathode materials for intermediate temperature SOFC, the mixed conducting $LnBaCo_{2-x}Fe_xO_{5+\delta}$ (Ln = Nd and Gd) oxides with a layered perovskite structure have been investigated. The air-synthesized $NdBaCo_{2-x}Fe_xO_{5+\delta}$ samples adopt a tetragonal structure (space group: $P4/mmm$) for $0 \le x \le 1.0$ and a cubic structure (space group: $Pm\text{–}3m$) for $1.5 \le x \le 2.0$. On the other hand, the air-synthesized $GdBaCo_{2-x}Fe_xO_{5+\delta}$ samples have an orthorhombic structure (space group: $Pmmm$) for $x = 0$ and a tetragonal structure (space group: $P4/mmm$) for $0.5 \le x \le 1.0$. The oxygen content and the oxidation state of (Co, Fe) increase, while the TEC and electrical conductivity decrease with increasing Fe content in $LnBaCo_{2-x}Fe_xO_{5+\delta}$ (Ln = Nd and Gd). The $x = 0.5$ samples show slightly improved cathode performances while a further increase in Fe content leads to a decrease in performance as has been found with disordered perovskite systems. Considering the TEC value, chemical stability with the electrolyte, and catalytic activity for ORR, the $x = 0.5$ sample represents an optimum composition in the $LnBaCo_{2-x}Fe_xO_{5+\delta}$ (Ln = Nd and Gd) system for use as a cathode in intermediate temperature SOFC.

Acknowledgement

Financial support by the Welch Foundation grant F-1254 is gratefully acknowledged.

References

[1] R.A. De Souza, J.A. Kilner, Solid State Ionics 106 (1998) 175.

[2] H. Yokokawa, T. Horita, in: S.C. Singhal, K. Kendall (Eds.), High Temperature Solid Oxide Fuel Cells: Fundamentals, Designs and Applications, Elsevier, Oxford, 2003, p. 127.
[3] J.-H. Kim., F. Prado, A. Manthiram, J. Electrochem. Soc. 155 (2008) B1023.
[4] I.O. Troyanchuk, N.V. Kasper, D.D. Khalyavin, Phys. Rev. B 58 (1998) 2418.
[5] C. Frontera, A. Caneiro, A.E. Carrillo, J. Oró-Solé, J.L. García-Muñoz, Chem. Mater. 17 (2005) 5439.
[6] J.C. Burley, J.F. Mitchell, S. Short, D. Miller, Y. Tang, J. Solid State Chem. 170 (2003) 339.
[7] G. Kim, S. Wang, A.J. Jacobson, L. Reimus, P. Brodersen, C.A. Mims, J. Mater. Chem. 17 (2007) 2500.
[8] J.-H. Kim, A. Manthiram, J. Electrochem. Soc. 155 (2008) B385.
[9] L.A. Chick, L.R. Pederson, G.D. Maupin, J.L. Bates, L.E. Thomas, G.J. Exarhos, Mater. Lett. 10 (1990) 6.
[10] H. Taguchi, D. Mastuda, M. Nagao, K. Tanihata, Y. Miyamoto, J. Am. Ceram. Soc. 75 (1992) 201.
[11] J. Rodriguez-Carjaval, Physica B 192 (1993) 55.
[12] A. Manthiram, J.S. Swinnea, Z.T. Sui, H. Steinfink, J.B. Goodenough, J. Am. Chem. Soc. 109 (1987) 6667.
[13] L.J. Van der Pauw, Philips Res. Rep. 13 (1958) 1.
[14] I. Reiss, J. Appl. Phys. 71 (1992) 4079.
[15] J. Wan, J.H. Zhu, J.B. Goodenough, Solid State Ionics 177 (2006) 1211.
[16] P. Karen, J. Solid State Chem. 177 (2004) 281.
[17] J. Lindén, P. Karen, A. Kjekshus, J. Miettinen, T. Pietari, M. Karppinen, Phys. Rev. B 60 (1999) 15251.
[18] R.D. Shannon, Acta Crystallogr. A32 (1976) 751.
[19] K.T. Lee, A. Manthiram, Solid State Ionics 176 (2005) 1521.
[20] M.W. Chase Jr., C.A. Davies, J.R. Downey Jr., D.J. Frurip, R.A. McDonald, N. Syverud, J. Phys. Chem. Ref. Data 118 (Suppl. 1) (1985) 926.
[21] M.A. Señarís-Rodríguez, J.B. Goodenough, J. Solid State Chem. 118 (1995) 323.
[22] K. Huang, H.Y. Lee, J.B. Goodenough, J. Electrochem. Soc. 145 (1998) 3220.
[23] C. Frontera, J.L. García-Muñoz, A. Llobet, Ll. Mañosa, M.A.G. Aranda, J. Solid State Chem. 170 (2003) 349.
[24] H. Takahashi, F. Munakata, M. Yamanaka, Phys. Rev. B 57 (1998) 15211.
[25] K.-T. Lee, A. Manthiram, Chem. Mater. 18 (2006) 1623.
[26] V.V. Kharton, F.M.B. Marques, A. Atkinson, Solid State Ionics 174 (2004) 135.
[27] J.-H. Kim, L. Mogni, F. Prado, A. Caneiro, A. Manthiram, J. Electrochem. Soc. 156 (2009) B1376.
[28] J.R. Wilson, W. Kobsiriphat, R. Mendoza, H.-Y. Chen, J.M. Hiller, D.J. Miller, K. Thornton, P.W. Voorhees, S.B. Adler, S. Barnett, Nat. Mater. 5 (2006) 541.
[29] Y. Teraoka, H.-M. Zhang, S. Furukawa, N. Yamazoe, Chem. Lett. (1985) 1743.
[30] T. Ishihara, T. Yamada, H. Arikawa, H. Nishiguchi, Y. Takita, Solid Sate Ionics 135 (2000) 631.